

Synthesis and characterization of microwave-assisted TiO₂ nanoparticles for dye-sensitized solar cell application

PRIYANKA ARUN, T. RAGURAM, P. MALAVIKA MENON, P. J. SAJNA, K. S. RAJNI*

Dept. of Sciences, Amrita School of Engineering, Coimbatore, Amrita Vishwa Vidyapeetham, India

In the present work, microwave-assisted TiO₂ nanoparticles are prepared by varying the pH (3, 5 and 7) of the precursor solution. XRD results show a mixture of anatase and rutile phases. Microstructural analysis calculated for the peak (110) shows the crystallite size of 7 to 11 nm. From UV-DRS studies, a strong absorption is found at 415 nm and it is blue-shifted when the pH is increased from 3 to 7 and bandgap varies from 4.2 to 3.0 eV. From FTIR spectral analysis, the bending vibrations of Ti-O and Ti-O-Ti are confirmed. PL spectrum shows excitonic emission band and O₂⁻ vacancies at 440, 467, 532 and 542 nm. DSSC is fabricated with Eosin Blue as the sensitizer and TiO₂ working electrode, the efficiency is found to be 1.60%.

(Received November 11, 2019; accepted October 21, 2020)

Keywords: DSSC, TiO₂, Microwave, XRD, Optical, J-V

1. Introduction

The appreciable conversion efficiency and low-cost fabrication technique of DSSC led to widespread attention in the field of solar cells. The conventional DSSC consists of photoanode sensitized with light-absorbing dye, platinum counter electrode sandwiched with I⁻/I₃⁻ redox electrolyte as an electron-hole transporter [1]. The d-block metal-oxides like TiO₂, SnO₂, VO₂, and ZnO have been extensively used as photoelectrodes due to their tunable bandgap and unique structural and textural properties. Among them, the TiO₂ photoanode is most commonly used in DSSC. Though the bandgap of TiO₂ (E_g > 3 eV) has limited the application of solar cell due to its high absorption only in the UV region, Gratzel and workers made a breakthrough in the solar cells by using the porous structure nature of the materials which results in the high surface area and favors the high dye loading and improving the current density of DSSC. Also TiO₂ exhibits no optical corrosion and is less toxic. In DSSC, the increased efficiency is due to the highly porous structure which enhances higher light scattering effect and hence enhances the light-harvesting efficiency. It is noted that the physicochemical properties of TiO₂ vary with the size and morphology of the synthesized particle. Studies are carried out in tuning the optical bandgap of TiO₂ and in reducing the electron-hole recombination by controlling the defects in TiO₂. Strong interface bonding of TiO₂ thin film photoanode is maintained by chemical treatment of precursor (Titanium tetraisopropoxide) [1]. TiO₂ exists in rutile (tetragonal), anatase (tetragonal) and brookite (orthorhombic) phase. The anatase and rutile phases are used for DSSC applications and anatase phase is mostly preferred as the resistance of rutile phase increases at high temperature during cell fabrication process which results

in decreasing the photocurrent. The usual preparation of TiO₂ includes sol-gel technique [2], hydrothermal method [3], hydrolysis approach [4], solvothermal method [5], direct oxidation method [6], chemical Vapour deposition [7], electrodeposition [8], sonochemical method [9] and microwave method [10]. In the present work TiO₂ nanoparticles are synthesized by microwave method. The synthesis process are dependent on the interactions of the microwaves with the materials and the reaction medium, that is, under the action of the electromagnetic field, the particles can produce different types of polarization (electron, atom, orientation, and space charge), being the microwave energy transmitted directly to the material in terms of molecular interactions with the electromagnetic field, leading to a fast and homogenous heating process in short periods of time and generating a homogeneous nucleation and a uniform growth of the nanoparticles [11]. The advantage of this method is the nanoparticles obtained are with desired crystallinity and good dispersibility and there are no additional stabilizing agents required which avoid contamination. Also in microwave-assisted technique, the heating process is rapid, uniform and efficient and hence reduce reaction time. The decrease in the reaction time and temperature restrict particle growth, improve uniformity of microstructure and higher chemical yield [12].

The effect of pH on the synthesis of nanoparticles, the stability of cluster distribution and colloid formation is increased with a declined tendency for aggregation of the particles due to complete charging of the clusters which maximize the repulsive electrostatic/electrosteric interactions. At elevated, monodispersed and small spherical nanoparticles are formed as well as the amount of nanoparticles was also higher. A possible reason for this result was that during the elevated pH, the reaction rate

will be increased with subsequent crystallization into smaller particles, which involved the nucleation and growth processes of smaller particles from parent nuclei [13].

In DSSC, numerous dye sensitizers including ruthenium complexes and metal-free organic dyes, toward broad absorption in the spectral range between 300 and 800 nm, have been designed and synthesized for their uses in DSSC [14]. The ideal dye sensitizer for the DSSC achieved 11% obtained from N719, while the highest efficiency for metal-free organic dyes has been reported to be 8% [14]. Some of the metal-free organic dyes are xanthenes, coumarin, porphyrins and indolines [15, 16], are also highly competitive candidates for use as sensitizers for DSSCs owing to their high molar excitation extinction coefficient, easy preparation, low cost, and complicated structures. These dye structures all can provide COOH based anchoring group for connecting the TiO₂ surface. Compared to Ru based complexes, the above mentioned organic dyes, in most cases, have only one anchoring group, which should affect the fixation of dye on TiO₂ surface [14]. Organic xanthene dye (Eosin Y) can well satisfy these thermodynamic requirements and provide enough driving force for both electron injection and dye regeneration [14]. Although the device conversion efficiency based on eosin Y was still low. In the present work, Eosin Blue dye used as sensitizer for DSSC. Eosin Blue is a dibromo-dinitro derivative of fluorescein with -COOH functional group and is responsible for anchoring the dye with TiO₂ and the absorption of light [17].

2. Experimental technique

2.1. Preparation of TiO₂ nanoparticles by Microwave-Assisted method

To 0.01 M NaOH (0.01g of NaOH in 25 mL of distilled water), 2.5 mL of Titanium tetraisopropoxide was added under vigorous stirring and pH is maintained at 7 (Sample 3). The obtained white-colored solution was heated in a microwave oven set at 150°C for 5 minutes. A white color precipitate was obtained and it was grinded to powder form. This powder was then annealed in a muffle furnace at 300°C for 3 hours. Two more samples were prepared by varying the pH (pH 5-sample 2 and pH 3-sample1) and the procedure was repeated.

2.2. Fabrication of DSSC

TiO₂ photoanode was prepared by mixing synthesized TiO₂ NPs with few drops of Triton X-100 and acetylacetone. The prepared paste was coated onto the well-cleaned FTO substrate (0.5 × 0.5 cm) by the Doctor Blade technique and it was annealed at 450 °C for 45 minutes in the air atmosphere. Eosin Blue dye solution was prepared by adding 2.3 mg of Eosin Blue with 2.3 mL of ethanol and 2.5 mL of Acetonitrile. Further, the

prepared photoanode was soaked into the Eosin blue dye solution for 48 hours. The redox electrolyte ($[I_3^-]/[I^-]$) was prepared by dissolving 0.5 M Lithium iodide (Sigma Aldrich) and 0.05 M Iodine (Nice) in acetonitrile (Himedia) in the ratio of 1:9. The platinum counter electrode (0.5 × 0.5 cm) was prepared from 5 mM of Chloroplatinic acid (H₂PtCl₆) [Sigma Aldrich] in acetonitrile onto finely cleaned FTO substrate by electrodeposition technique with an applied potential of -0.4 V for 120 seconds. After deposition, the platinum counter electrode was kept in hot air oven at 100 °C for one hour. The cell was fabricated by placing a dye-sensitized TiO₂ photoanode on top of the Pt counter electrode and these two electrodes were separated by paraffin and clamped tightly together with the binder clip. The prepared electrolyte was injected between the electrodes and it enters into the cell by capillary action. The fabricated device was placed towards the light source with a distance of 15 cm (1000 Lux) (Xenon lamp).

2.3. Characterization

The structural analysis was carried out by an X-ray diffractometer (Rigaku Ultima IV) with CuK α radiation of wavelength ($\lambda = 1.541 \text{ \AA}$). The optical analysis was carried out UV-DRS spectrophotometer (UV 2600 ISR) in the wavelength range of 200 – 700 nm. The functional groups of the sensitizers were analyzed using FTIR by KBr pellet technique (Perkin Elmer spectrophotometer) in the range of 4000 – 400 cm⁻¹. The surface morphology and elemental analysis of the prepared sample were assessed by SEM (Scanning Electron microscopy) with EDS (Energy Dispersive X-ray Analysis) (ZEISS). The photoluminescence (PL) spectra of the TiO₂ photoanodes were taken by fluorescence spectrophotometer (RF 6000). The J -V characteristics of DSSC were measured by Keithley instrument (2450 source meter).

3. Results and discussion

3.1. Structural analysis

The powder X-ray Diffraction analysis of microwave synthesized TiO₂ nanoparticles at various pH are shown in Fig. 1. From XRD analysis, it is noted that the TiO₂ nanoparticles show tetragonal structure with the planes (101), (110), (004), (200), (213), (215), (303) and *(211), (301) matches well with the anatase (JCPDS Card No. 89-4203) and *rutile (JCPDS Card No 87-0920) phase of the TiO₂. The observations show that at low pH, both rutile and anatase phase exists and as the pH increases the anatase phase becomes dominant. Microstructural analysis calculated for the prominent rutile anatase peak (101) is shown in Table 1. The crystallite size, calculated by Scherer equation Eqn. (1) is found to be increasing with pH and the values are shown in Fig. 2. The strain-induced broadening in powders, due to crystal imperfection and distortion is calculated using the formula (2) [18].

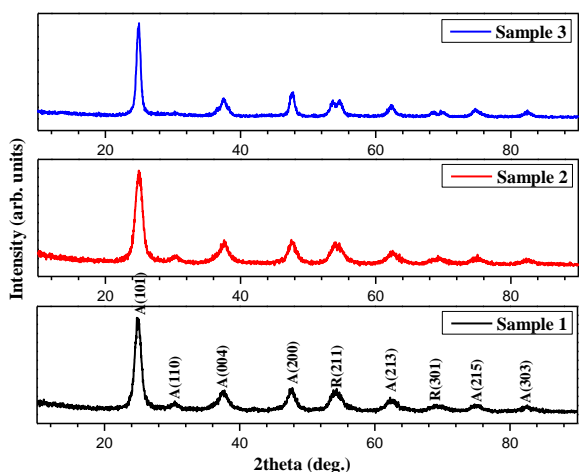


Fig. 1. XRD Pattern of TiO₂ nanoparticles by microwave synthesis method at various pH (color online)

$$D = \frac{k\lambda}{\beta \cos \theta} \quad (1)$$

$$\varepsilon = \frac{\beta \cos \theta}{4} \quad (2)$$

The strain decreases with the increases in the crystallite size and the lattice constant and the d-spacing is close to the standard value for TiO₂ nanoparticles. One of the prominent characteristics of nanoparticles is that they tend to float in solution and they need much longer time to be precipitated in as much as the gravitation force exerting them is very small, or even almost negligible [19]. It was hypothesized that by varying the pH condition, the size of the particle obtained would also be varied, and this would affect the precipitation profile of the TiO₂ nanoparticles [20].

Table 1. Microstructural parameters of the prepared particles by Microwave-Assisted method at various pH

Sample code	d- spacing (Å)	Crystallite size (D) (nm)	Lattice Constant (Å) a = 3.785 c = 9.514	Microstrain
1	3.4497	7.60	a= 3.7803 c = 9.4592	0.1067
2	3.4839	8.55	a = 3.7713 c = 9.4505	0.1060
3	3.4950	11.81	a = 3.7799 c = 9.5146	0.0067

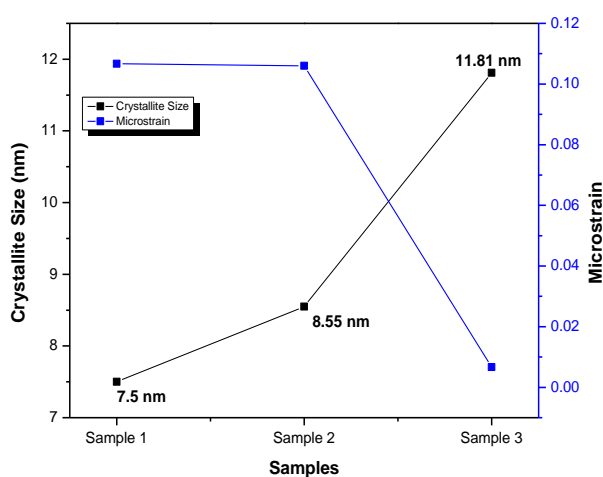


Fig. 2. Crystallite size Vs Microstrain at various pH (color online)

Table 1 shows the Microstructural analysis of synthesized nanoparticles. From the table the crystallite sizes are found to be 7.60 (pH 3), 8.55 (pH 5) and 11.81 (pH 7) nm, respectively and It is in agreement with hypotheses above that as pH of the solution increased, the

size of the nanoparticle increased as well. Observation shows that the pH value of the microwave synthesis is a decisive factor for controlling the final particle size, shape, phase and agglomeration [21].

3.2. Functional group analysis (FTIR)

FTIR study involves examination of stretching, bending, twisting and vibrational modes of an atom in a molecule and hence to detect the functional groups which are present in the prepared samples. The recorded FTIR spectrum is shown in Fig. 3. The broad envelope in the higher wavenumber region of 3401 cm⁻¹ is due to OH stretching bonds. The peaks observed around 1616 cm⁻¹ are assigned to C = O stretching vibration. The peaks in the region 1408 cm⁻¹ for the samples are due to CH₃ deformation. The COO⁻ group in carboxylic acid is found to be around 1321 cm⁻¹ [22]. In the low energy region of the spectrum, the band at 440 cm⁻¹ is assigned to bending vibrations of Ti-O and Ti-O-Ti framework bonds [23]. The above results confirm the presence of pure TiO₂ nanoparticles vibrations of Ti-O and Ti-O-Ti framework bonds [23]. The above results confirm the presence of pure TiO₂ nanoparticles.

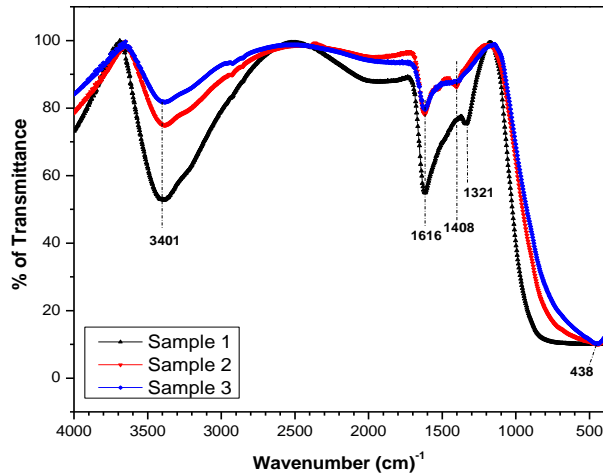


Fig. 3. FTIR Spectra of TiO_2 nanoparticles by microwave synthesis method at various pH (color online)

3.3. Optical analysis – UV-DRS

UV - DRS studies give details about the structure of the molecules. This is due to the absorption of UV and visible light which affects the electron transfer in σ and π orbitals from lower to higher energy states. The reflectance spectra of TiO_2 nanoparticles at various pH were recorded in the 200–700 nm region is shown in Fig. 4. The reflectance is started at 415 nm for the prepared samples which is due to the strong absorption. The absorption edge is gradually blue-shifted when pH increases from 3 to 7. The blue shift in the band edge is a consequence of exciton confinement and confirms the presence of nanoparticulate materials. Due to confinement of both electrons and holes, the lowest energy optical transition from the valence to conduction band will increase in energy, effectively increasing the band gap [24]. The bandgap was calculated using Kubelka-Munk relation, to convert the reflectance into a Kubelka-Munk function (which is equivalent to the absorption coefficient), $F(R_\infty)$, using the relation [25]:

$$F(R_\infty) = \frac{(1-R_\infty)^2}{2R_\infty} \quad (3)$$

where R_∞ is the reflectance of an infinitely thick sample with respect to a reference at each wavelength. Fig. 5 (a), (b) and (c) shows the Kubelka-Munk plots for prepared samples and the bandgap values are found to be 3.05 eV (sample 1), 3.95 (sample 2) and 4.01 eV (sample 3) with an indirect transition [25].

3.4. Photoluminescence analysis

PL spectrum is used to determine the performance of photo-generated electrons and holes in the semiconductor layer of DSSCs [26]. The position of the luminescence peaks is associated with the crystalline structure and the oxygen vacancies of the samples [27]. PL emission spectra are recorded for all the samples in the range of 350–600 nm with the excitation wavelength at 350 nm (Fig. 6 (a), (b) and (c)). The PL spectrum shows three visible emission peaks and the peaks at 397 and 414 nm are due to the excitonic emission band. The peaks at 440, 467, 532 and 542 nm are due to O_2^- vacancies. The maximum emission intensity is obtained at sample 1 (pH 3) which may be due to the less electron-hole recombination pairs. A low PL emission intensity indicates the improved charge separation and the electron transfer can effectively decrease the recombination of charge [28].

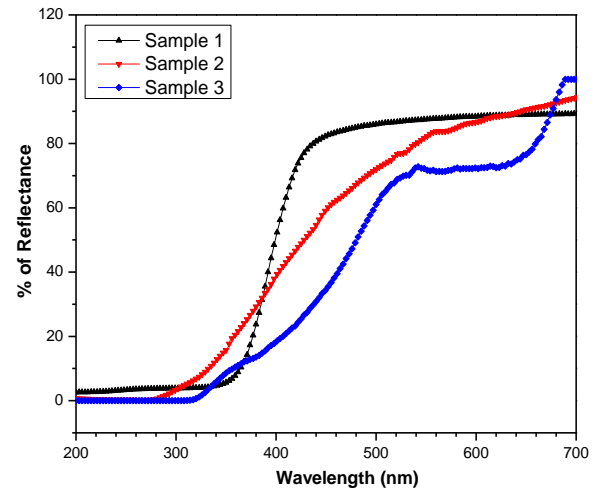


Fig. 4. UV-DRS Spectra of TiO_2 nanoparticles by microwave synthesis method at various pH (color online)

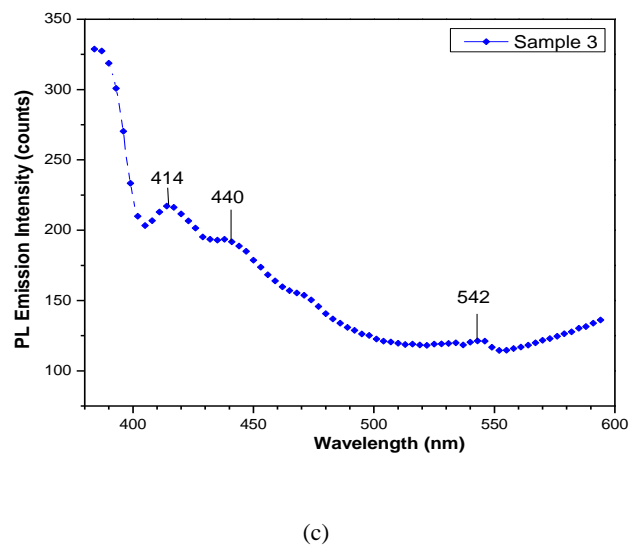
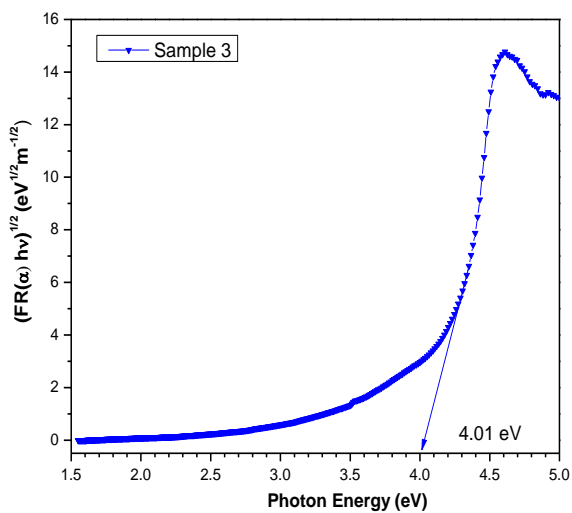
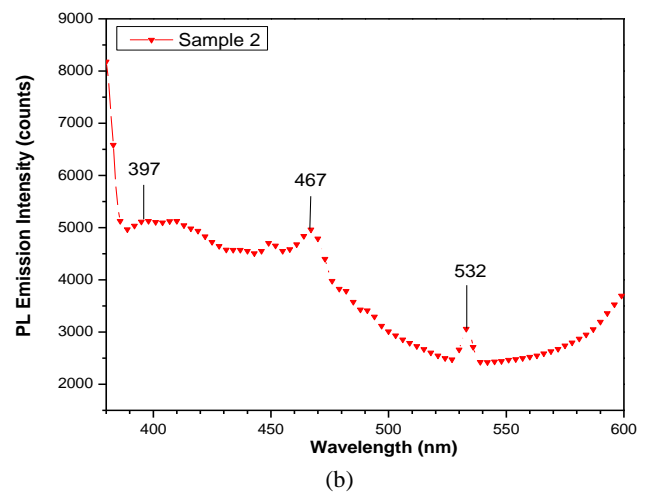
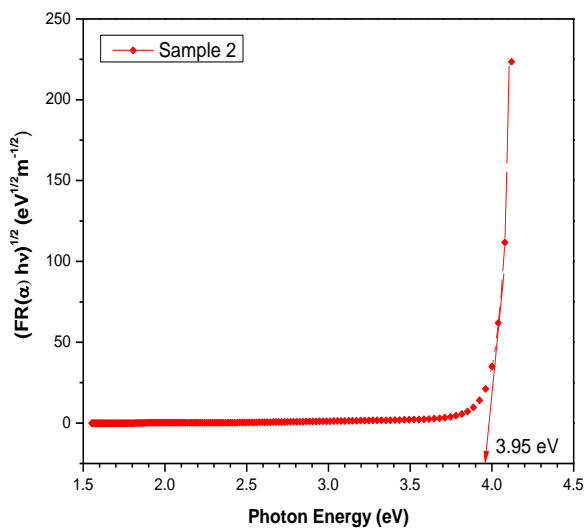
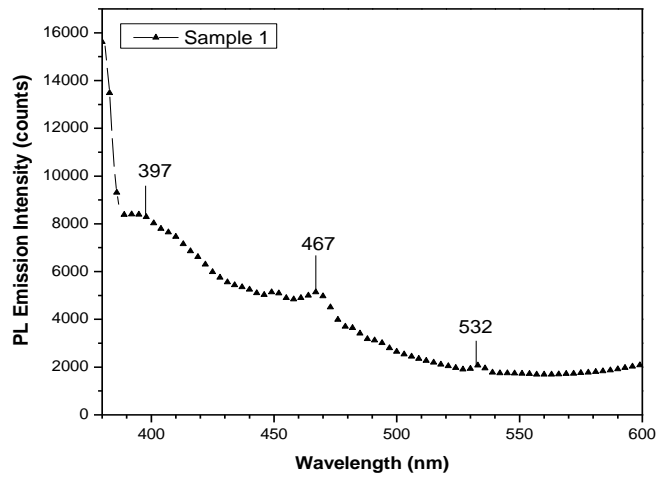
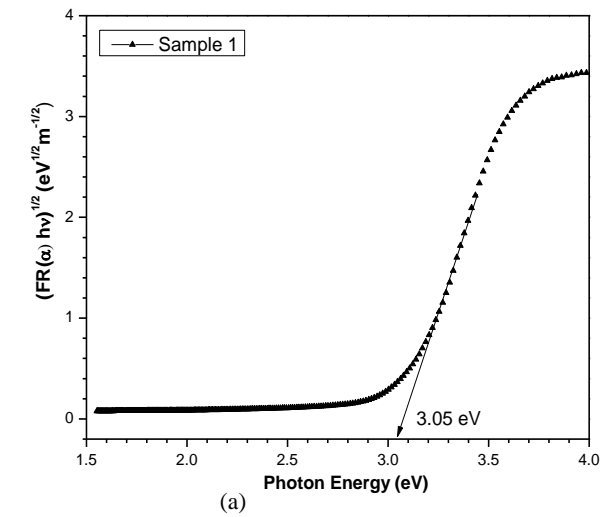


Fig. 6. (a), (b) and (c) PL Emission spectra of TiO₂ nanoparticles by microwave synthesis method at various pH

Fig. 5. (a), (b) and (c) Kubelka-Munk plots of TiO₂ nanoparticles by microwave synthesis method at various pH

3.5. Morphological and Compositional Analysis

The SEM image of the prepared sample is shown in Fig. 7. It is noted that the particles are spherical in shape and its agglomerates due to the high surface area [29]. The morphology of the sample prepared with ethanol as the solvent is striking, as the sample is made of very spherical agglomerations of smaller crystallites. As the morphology of the nanostructures could be controlled reliably using microwave synthesis. The particle size of the sample 1 is ~ 15 nm using ImageJ software. The corresponding EDS spectra show the presence of only titanium and oxygen (Fig. 8). Moreover, the semi-quantitative analysis shows 52.67 wt% of Ti and 47.09 wt% of O (Fig. 8) which indicates the purity of materials [30].

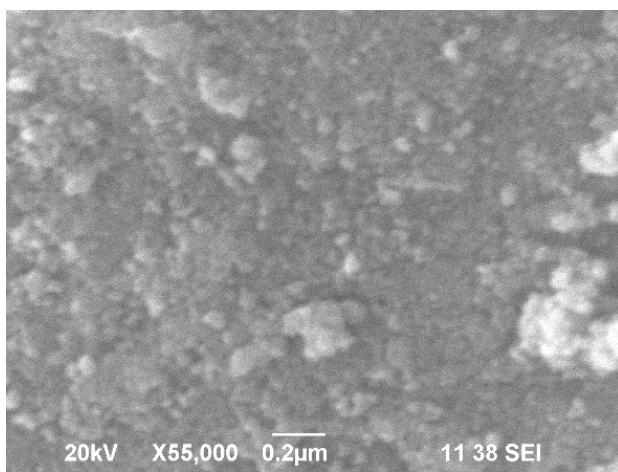


Fig. 7. SEM image (sample 1) of TiO_2 nanoparticles by microwave synthesis method

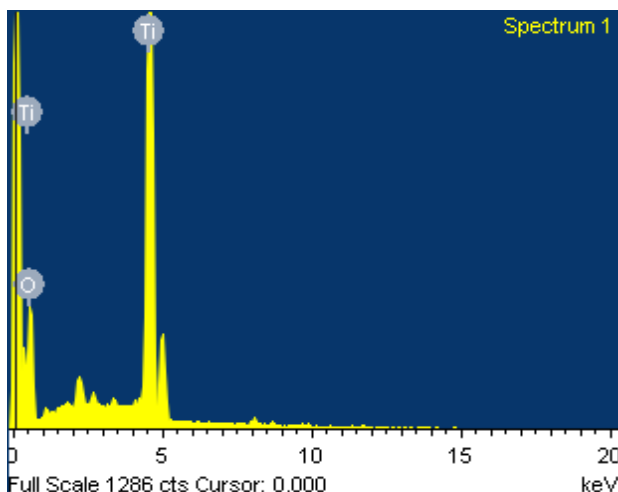


Fig. 8. EDS spectrum (sample 1) of TiO_2 nanoparticles by microwave synthesis method (color online)

3.6. J – V analysis

J - V characteristics of the prepared Eosin blue sensitized TiO_2 photoanode (sample 1 – pH 3) are shown

in Fig. 9. The fill factor (FF) and efficiency (η) are denoted by the formulae [31]

$$FF = \frac{J_{max} * V_{max}}{J_{sc} * V_{oc}} \quad (4)$$

$$\eta = \frac{J_{sc} * V_{oc} * FF}{P_{in}} \quad (5)$$

where J_{sc} is the short circuit current density (mA cm^{-2}), V_{oc} is the open-circuit voltage (volts), Power input (P_{in}) is the intensity of the incident light ($P_{in} = 100 \text{ mW cm}^{-2}$), J_{max} is the maximum current density and V_{max} is the maximum voltage obtained from J-V curve. When the dye molecules absorb photon from the source, the dye electron excited from HOMO to LUMO of the dye. Then the electrons are injected into the conduction band of TiO_2 then to the back contact towards FTO. Further the electrons are transferred via load to the Pt coated FTO. The excited dye molecules are regenerated from the redox electrolyte. The oxidized electrolyte then diffuses towards to the Pt counter electrodes and then it is reduced. Table 2 shows the solar cell parameters of sensitized photoanode based DSSC. Under illumination, the device exhibits a short-circuit current density (J_{sc}) of 8.99 mA cm^{-2} , an open-circuit voltage (V_{oc}) of 0.390 mV and a fill factor (FF) of 0.46 , resulting in the overall conversion efficiency of 1.60% .

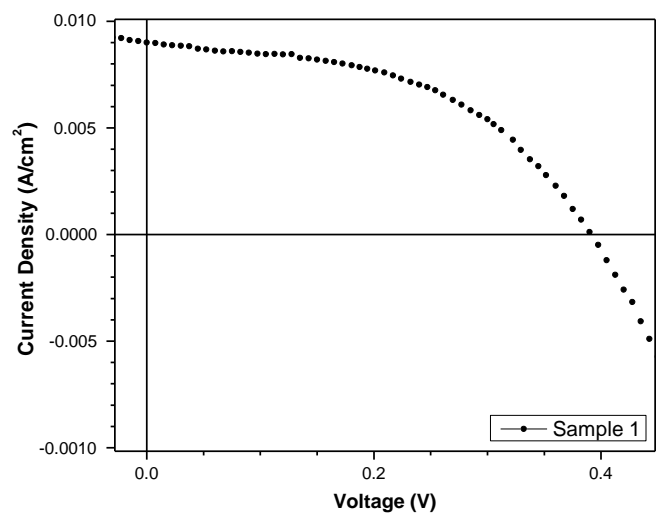


Fig. 9. J – V characteristics of Eosin Blue sensitized TiO_2 photoanode (sample 1 – pH 3)

Table 2. J - V parameters of the Eosin blue sensitized TiO_2 photoanode (sample 1 – pH 3)

Sample Code	J_{sc} (mA cm^{-2})	V_{oc} (V)	FF (%)	η (%)
Sample 1	8.99	0.3900	0.46	1.60

4. Conclusion

TiO₂ nanoparticles are synthesized by the microwave-assisted method was carried out at different pH. The prepared TiO₂ powder was subjected to annealing temperature of 300°C for 3 hours. Based on XRD results, both the anatase and rutile were observed in all the prepared samples and with increase in PH, the peaks become prominent. From the Microstructural analysis the crystallite size was found to be 7.6 to 11.8 nm. From FTIR spectral analysis the bending vibrations observed at 440 cm⁻¹ confirms the presence of TiO₂. From UV-DRS studies, the strong absorption observed at 415 nm is blue-shifted when the pH increases from 3 to 7. The bandgap calculations show that the transitions are indirect allowed and the bandgap was found to increase from 3.05 to 4.01 when the pH increases from 3 to 7. PL spectrum shows excitonic emission band and O₂⁻ vacancies at 440, 467, 532 and 542 nm. From J-V characteristics, the solar cell parameters J_{sc}, V_{oc}, FF, and efficiency are found to be 8.99 mA cm⁻², 0.390 V, 0.46 and 1.60%.

Acknowledgments

The authors acknowledge to Dr. M Karthega, Assistant Professor, Amrita Material Science Lab., and Dr. Sudip K. Batabyal, Senior Research Scientist, Amrita Nanomaterial Research Laboratory and Dr. T. G. Satheesh Babu, Associate Professor, Biosensor Research Laboratory, Amrita Vishwa Vidyapeetham, Coimbatore, India, for providing lab facilities and their constant support.

References

- [1] Md. Mosaddeq-ur-Rahaman, K. Murali Krishna, Takeshi Miki, Tetsuo Miki, Tetsuo Soga, Kazuo Igarashi, Sakae Tanemura, Masayoshi Umeno, *Sol. Energy Mater. Sol. Cells* **48**(14), 123 (1997).
- [2] Guangshe Li, Liping Li, Juliana Boerio-Goates, Brian F. Woodfield. *J. Am. Chem. Soc.* **127**(24), 8659 (2005).
- [3] D. Reyes-Coronado, G. Rodriguez-Gattorno, M. E. Espinosa-Pesqueira, C. Cab, R. De Coss, G. Oskam, *Nanotechnology* **19**, 145605 (2008).
- [4] W. F. Zhang, Y. L. He, M. S. Zhang, Z. Yin, Q. Chen, *J. Phys. D: Appl. Phys.* **33** (8), 912 (2000).
- [5] R. K. Wahi, Y. Liu, C. J. Falkner, V. L. Colvin, *J. Coll. Int. Sci.* **302**, 530 (2006).
- [6] W. H. Ryu, C. J. Park, H. S. Kwon, *J. Nano and Nanotechnology* **8**, 1 (2008).
- [7] P. S. Shinde, C. H. Bhosale, *J. Anal. Appl. Pyrolysis* **82**, 83 (2008).
- [8] W. Tan, J. Chen, X. Zhou, J. Zhang, Y. Lin, X. Li, X. Xiao, *J. Solid. State. Electrochem.* **13**, 651 (2009).
- [9] H. Arami, M. Mazloumi, R. Khalifehzadeh, S. K. Sadrnezhaad, *Mat. Let.* **61**, 4559 (2007)
- [10] A. B. Corradi, F. Bondioli, B. Focher, A. M. Ferrari, C. Grippo, E. Mariani, C. Villa, *J. Am. Ceram. Soc.* **88**(9), 2639 (2005).
- [11] G. S. Falk, M. Borlaf, M. J. López-Muñoz, J. C. Fariñas, J. B. Rodrigues Neto, R. Moreno, J. *Nanopart. Res.* **20**, 23 (2018).
- [12] Gema Cabello, Rogério A. Davoglio, Ernesto C. Pereira, *J. Electroanal. Chem.* **794**(1), 36 (2017).
- [13] Lakkappa B Anigol, Jasmith S Charantimath, Prabhuodeyara M Gurubasavaraj, *Organic & Medicinal Chem IJ*, **3** (5): OMCIJ.MS.ID.555622 (2017).
- [14] Yan Fang Zhou, Xue Ping Li, Jing Bo Zhang, Xiao Wen Zhou, Yuan Lin, *Chinese Science Bulletin* **54**(15), 2633 (2009).
- [15] D. El Mekkawi, M. S. A. Abdel-Mottaleb, *J. Photoenergy* **7**, 95 (2005).
- [16] T. Horiuchi, H. Miura, S. Uchia, *J. Photoch. Photobio. A* **164**, 29 (2004).
- [17] Y. Akila, N. Muthukumarasamy, S. Agilan, S. Senthilarasu, Dhayalan Velauthapillai, *Appl. Phys. A* **122**, 719 (2016).
- [18] P. Bindu, Sabu Thomas, *J. Theor. Appl. Phys.* **8**(4), 123 (2014).
- [19] B. Sunandan, D. Joydeep, *J. Cryst. Growth* **318**(8), 2549 (2009).
- [20] Radium Ikono, Putri Riskia Akwalia, Siswanto, W. Wahyu Bambang, Agus Sukarto, Nurul Taufiq Rochman, *International Journal of Engineering and Technology* **12**(6), 5 (2012).
- [21] V. Biju, N. Sugathan, N. Vrinda, S. L. Salini, *J. Mater. Sci.* **43**(4), 1175 (2008).
- [22] Joseph B. Lambert et al., *Introduction to Organic Spectroscopy*, Macmillan Publ. New York, 1987.
- [23] M. Picquart, L. Escobar-alarcon, E. Torres, T. Lopez, E. Haro-Poniatowski, *J. Mater. Sci.* **37**(15), 3241 (2002).
- [24] Damian C. Onwudiwe, Peter A. Ajibade, *Int. J. Mol. Sci.* **12**(9), 5538 (2011).
- [25] Mou Pal, Umapada Pal, Justo Miguel Gracia Y. Jimenez, Felipe Perez-Rodriguez **7**, 1 (2012).
- [26] Siti Zubaidah Siddick, Chin Wei Lai, Joon Ching Juan, *Mat. Sci. Semicon. Proc.* **74**, 267 (2018).
- [27] S. Arunmetha, V. Rajendran, M. Vinoth, A. Karthik, S. R. Srither, M. Srither Panday, N. Nithyavathy, P. Manivasakan, M. Maaza, *Mater. Res. Express* **4**, 035016 (2017).
- [28] Moges Tsega, F. B. Dejene, *Heliyon* **3**, e00246 (2017).
- [29] Anirudha Jena, R. Vinu, S. A. Shivashankar, M. Gridhar, *Ind. Eng. Chem. Res.* **49**(20), 9636 (2010).
- [30] M. Andre-Guel, L. Diaz-Jimenez, D. Cortes-Hernandez, C. Cabello-Alvarado, C. Avila-Orta, P. Bartolo-Perez, P. Gamero-Melo, *Bol. Soc. Esp. Ceram V.* **58**(4), 171 (2019).
- [31] T. S. Senthil, N. Muthukumarasamy, Dhayalan Velauthapillai, S. Agilan, M. Thambidurai, R. Balasundaraprabhu, *Renewable Energy* **36**(9), 2484 (2011).

*Corresponding author: ks_rajani@cb.amrita.edu